Design and Modelling of Solidly-Mounted Resonators for Low-Cost Particle Sensing

Farah Helue Villa-López[a], Girish Rughoobur[b], Sanju Thomas[a], Andrew J. Flewitt[b], Marina Cole[a], Julian W. Gardner[a]

[a] Microsensors and Bioelectronics Laboratory, University of Warwick, Coventry, UK, CV4 7AL
[b] Electrical Engineering Division, University of Cambridge, Cambridge, UK, CB3 0FA

Corresponding author: Julian W. Gardner, J.W.Gardner@warwick.ac.uk

Abstract **–** This work presents the design and fabrication of Solidly Mounted Resonator (SMR) devices for the detection of particulate matter (PM2.5 and PM10) in order to develop a smart low-cost particle sensor for air quality. These devices were designed to operate at a resonant frequency of either 870 MHz or 1.5 GHz, employing zinc oxide as the piezoelectric layer and an acoustic mirror made from molybdenum and silicon dioxide layers. Finite element analysis of the acoustic resonators was performed using COMSOL Multiphysics software in order to evaluate the frequency response of the devices and the performance of the acoustic mirror. The zinc oxide based acoustic resonators were fabricated on a silicon substrate using a five mask process. The mass sensitivity of the acoustic resonators was estimated using a 3-D finite element model and preliminary testing has been performed. The theoretical and observed mass sensitivity were similar at ca. 145 kHz/ng for the 870 MHz resonator when detecting PM2.5 suggesting that SMR devices have potential to be used as part of a miniature smart sensor system for airborne particle detection.

Keywords: Air quality monitoring, finite element model, particle sensor, solidly mounted resonator.

1. INTRODUCTION

Pollution is a common problem in both developed and developing countries and its effect on human health as well as environmental impact is an increasingly pressing concern. Particulate matter is one form of pollution that consists of discrete airborne particles and several studies have reported the adverse effects of airborne particulate matter on human health [1, 2]. These include a wide range of respiratory and cardiovascular health problems including: aggravated asthma, chronic bronchitis, decreased lung function and increased risk of myocardial infarction, which could lead to premature mortality in individuals with existing heart or lung problems.

Particulate matter is commonly grouped in two categories: PM10 and PM2.5. PM10 are defined as particles equal to and less than 10 µm in diameter, while PM2.5 are defined as fine particles and consist of particles equal to or less than 2.5 µm in diameter. The risk posed to human health as well as environmental impact of particulate matter means that methods are needed to measure and monitor concentrations of PM10 and PM2.5 in the ambient air.

The measurement of particulate matter concentrations is carried out using different methods. Filter-based gravimetric samplers collect particles from a sample air flow onto a filter, which is later sent to a laboratory in order to be weighed. For continuous monitoring of PM, automated mass measurement instruments, such as the tapered element oscillating microbalance (TEOM) collect particles onto an oscillating element, and its frequency shift is related to the particle mass. All these instruments, however, are complex, costly and large in size making them difficult for personal PM monitoring. Optical methods, mainly based on light scattering, are the most commonly used for particle detection, providing information about particle size and number of particles. However, even though optical based instruments are becoming smaller, they use assumptions about the characteristics of the particles (density, distribution) which make them less accurate.

Several works have reported the development of smaller fine particle sensors based on different operating principles. Devices based on the corona discharge principle were implemented by Lim et al. [3] and thermally actuated MEMS resonators with piezo resistive readout have been developed by Hajjam et al. [4] as particle sensors. Other works have reported the use of thin film piezoelectric on silicon resonators integrated within an aerosol impactor for the measurement of mass concentration of airborne particles [5] and the development of silicon resonant cantilever sensors for the detection of nanoparticles [6].

As an alternative approach, acoustic wave based devices, such as QCMs and SAW devices have been proposed to be employed in particle sensing, where the total mass of the particles deposited on the active area of the acoustic device is measured as a change in its resonant frequency. Early works have described an impactor instrument based on quartz crystal microbalance for the measurement of particles [7] and a particle mass sensing instrument was also developed by Bowers and Chuan using commercial delay line SAW devices [8]. More recent works have shown the utilisation of SAW resonators [9] and film bulk acoustic resonators as the mass-sensitive element for the detection of particulate matter [10, 11].

In this work we report on the design, modelling, fabrication and characterisation of zinc oxide based solidly mounted resonators for their application as miniature, portable, low-cost smart particle sensors for air quality monitoring. Prior to fabrication, the frequency response of the devices was modelled by finite element analysis and the sensitivity to particulate matter was estimated using a 3D finite element model. The initial characterisation of the fabricated devices is presented and preliminary experimental results are reported.

2. ACOUSTIC WAVE SENSORS

The sensing applications of acoustic wave based devices are very wide-ranging. These devices can serve, for instance, as gravimetric [12], temperature [13], pressure [14] and gas [15] sensors. These devices can also be used in biosensing and liquid phase sensing [16-20] and they can act as a chemical vapour sensors when a selective coating is used for the absorption of specific vapours [21, 22].

Two main types of acoustic wave devices can be defined as Surface Acoustic Wave (SAW) and Bulk Acoustic Wave (BAW) devices. In SAW devices, an electric signal applied to the input interdigital transducer (IDT) generates an acoustic wave that propagates along the surface of the substrate until it reaches the output IDT, where a mechanical to electrical conversion takes place and an electrical output is obtained. The characteristics of the propagating wave (amplitude, frequency, velocity or phase) are affected by the coupling between the components of the wave and the medium on the surface of the device. The typical operating frequencies of SAW devices are in the range of 30 MHz to 1 GHz [23].

Quartz Crystal Microbalances (QCM) are the most widely known bulk acoustic wave resonators. They commonly consist of an AT-cut quartz crystal (usually disk-shaped) with patterned metal electrodes on both sides. An electrical signal applied across the electrodes produces standing shear waves in the crystal. QCMs have been mainly used for gravimetric measurements, such as film thickness monitors in deposition processes. The mass sensitivity of QCMs is dependent on its resonant frequency, which in turn, is mainly determined by the thickness of the quartz crystal as shown in the Sauerbrey equation [24]:

$$\Delta f = \frac{2{f_0}^2}{\sqrt{\mu\rho}} \cdot \frac{\Delta m}{A} \tag{1}$$

where Δf is the change in resonant frequency, f_0 the fundamental resonant frequency, μ the elastic constant, ρ the density, Δm the mass load and A the surface area. The thinner the piezoelectric crystal,

the higher the resonant frequency and therefore the higher the sensitivity. However, thin quartz crystals are very fragile and therefore QCMs can only operate at frequencies typically in the range of 5 – 30 MHz [21]. Film bulk acoustic resonators (FBAR) use a thin piezoelectric layer sandwiched between two metal electrodes and fabricated on top a carrier substrate. Acoustic isolation to the substrate is achieved by creating an air gap between the substrate and the resonator structure [25].

Solidly mounted resonator (SMR) devices use an acoustic mirror, also known as Bragg reflector, for the wave energy confinement. The very first SMR structure was proposed by Newell [26]. In SMR devices, the acoustic mirror consisting of alternating layers of low and high acoustic impedance materials is deposited on top of a substrate, also typically silicon. The impedance mismatching between these layers causes a portion of the acoustic energy to be reflected at each interface of the multi-layered stack thus preventing energy leakage. Commonly used materials for the Bragg reflectors are SiO_2, aluminium and zinc oxide as low impedance materials while tungsten, aluminium nitride and molybdenum have been employed for the high-impedance layers. Large ratios of high to low acoustic impedance materials maximize the reflection [27] and thus, a smaller number of pairs is required. Figure 1 depicts the wave propagation through the structure of a solidly mounted resonator and the typical equivalent model of the SMR and driving circuitry.

In a recent work by Thomas *et al.* [9] a particle sensor based on SAW resonators was developed for the detection of fine particles with different sizes. A relationship between the mass sensitivity of the SAWR based sensor and the dimension of the particles was observed. This phenomenon was explained by the influence of the acoustic penetration depth of the SAWR, which is directly related to the resonant frequency of the device. Seeking the development of miniature and low-cost particle sensors, the utilisation of SMR devices is proposed in this work. In particular, we investigate the frequency response of the SMRs to the deposition of particles with different diameters to help developing tailored PM sensors based on SMRs operating at different frequencies.

As opposed to SAW devices, Solidly Mounted Resonators are compatible with silicon wafer processing technologies and suitable for low-cost monolithic integration. Furthermore, their smaller footprint, higher operating frequency, higher sensitivity, structural stability and good power handling capability make them a good candidate for the development of a high sensitive, low-cost particle sensor.

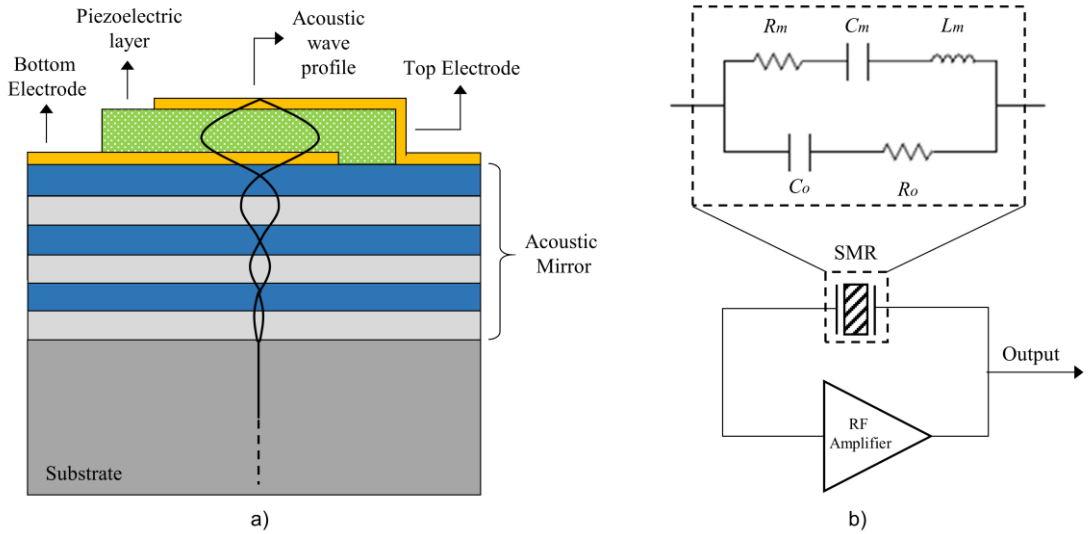

Figure 1. a) Wave propagation through the Solidly Mounted Resonator and acoustic mirror; b) Drive circuitry and equivalent circuit model of SMR devices.

The interaction of submicron-sized particles with different surfaces has become of great interest in areas such as nanotechnology and biology [28]. For the development of a particle sensor based on solidly mounted resonators, the interaction between the particles and the solid surface of the acoustic

device needs to be considered. Sauerbrey's equation (1) relates the resonance frequency of a QCM with the mass loading. However, this relationship only applies to thin rigid films firmly attached to the surface. Dybwad [29] developed a one-dimensional mechanical model of a solid particle in contact with the electrode's surface of a quartz resonator. In this model, the particle attached to the surface of the resonator forms a coupled oscillator system resonating at a new frequency. A strong particle binding to the surface will cause a decrease in the resonant frequency of the system leading to Sauerbrey equation. However, it was predicted that for a weak coupling, the resonant frequency of the system will increase. The same behaviour was observed in other works with a solid particle in contact with a thickness shear mode (TSM) sensor in air [28] and colloidal objects to the surface of a QCM in liquid phase media [30]. Further studies of the contact mechanics of particles with QCM devices and mathematical models have been carried out by Johannsmann [31, 32].

As the coupling strength of the particle-surface interaction is directly related to the particle size, negative frequency shift can be observed when the particles are small enough and positive frequency shift is predicted for larger particles. Therefore, the operating frequency of the resonator and the size of the particles deposited are factors to be taken into account when detecting particles.

3. DESIGN OF SOLIDLY MOUNTED RESONATORS

Solidly mounted resonators operating at frequencies of 870 MHz and 1.5 GHz were designed using zinc oxide as the piezoelectric material. For the acoustic mirror, molybdenum and silicon dioxide were used as the high acoustic impedance and low acoustic impedance layers, respectively. The devices were designed with two different electrode materials: aluminium or gold. The active area of the reported devices was designed to be 200 µm by 200 µm. The structure of the modelled solidly mounted resonators is shown in Figure 2(a). A cross section view of the devices showing all the layers is shown in Figure 2(b). The silicon substrate was assumed to be 500 µm thick as 4-inch silicon wafers would be used during fabrication. A thin 200 nm oxide layer is shown on top of the substrate as thermal oxide was grown on the silicon wafers in order to provide insulation. A total of 6 layers is used for the Bragg reflector. The piezoelectric material is deposited on top of the acoustic mirror and sandwiched between the bottom and top electrodes.

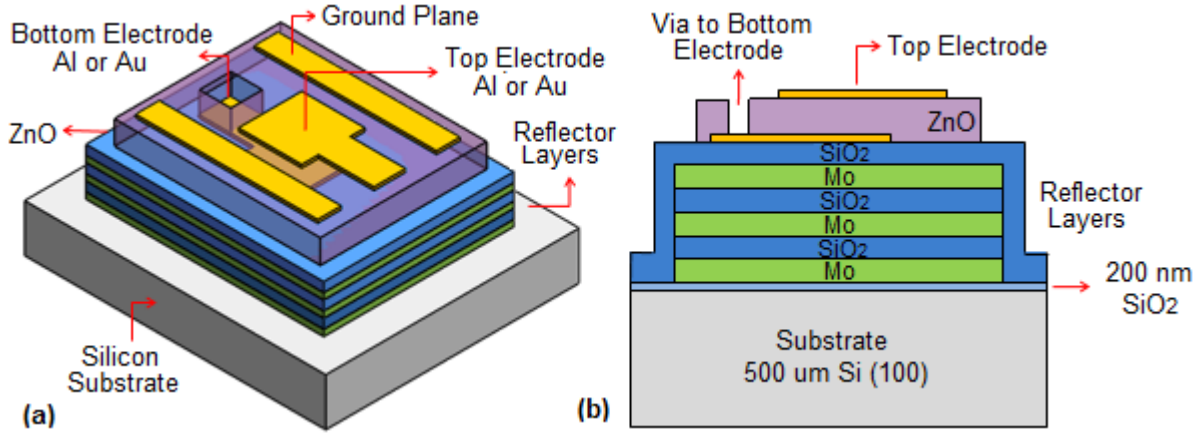

Figure 2. Structure of the designed solidly mounted resonators: a) 3-D representation and b) cross section of the devices illustrating the layers. Diagrams are not to scale.

The SMRs were incorporated within a coplanar waveguide (CPW) structure. In this configuration, the electrodes are connected to a short coplanar transmission line. The use of CPWs reduces parasitic effects and provides a ground-signal-ground configuration for a convenient method of making contact with the device [6]. The dimensions of the waveguide were determined in order to obtain a characteristic impedance of 50 Ω.

3.1. Theoretical Calculations

The SMR devices were designed using the half-wavelength mode configuration [33] in which the uppermost layer of the reflector stack is a low acoustic impedance layer. The acoustic reflector consisted on quarter wavelength layers. The thicknesses of the Mo/SiO_2 layer pairs were determined to be 1.82 µm/1.65 µm for the 870 MHz devices and 1.05 µm/995 nm for the 1.5 GHz devices.

The number of layer pairs of the reflector stack required to completely reflect back the wave into the resonator structure is determined by the acoustic impedance ratio of the materials used. Large ratios of high to low acoustic impedance materials maximize the reflection [27]. For the designed resonators, a total of six Mo/SiO_2 layer pairs were used with an acoustic impedance ratio of 5 to 1.

The half-wavelength thickness of the piezoelectric layer mainly determines the resonant frequency of the device. Thus, for a specific fundamental frequency, piezoelectric materials with higher acoustic velocities will lead to thicker films. Therefore, for the target frequencies of 870 MHz and 1.5 GHz, thinner zinc oxide layers are required thanks to its lower acoustic velocity compared, for instance, with aluminium nitride. The frequency response of SMRs is not only determined by the piezoelectric thickness but also by the characteristics of the electrodes, which need to be considered when designing the resonator. The selected metal and thickness of the top and bottom electrodes mainly affect the resonant frequency of the device as metal electrodes with higher densities decrease the resonant frequency as a result of the mass loading effect [34, 35]. The surface area of the electrodes does not affect the frequency response of the SMR [36] but it will have an influence on the sensitivity of the device for sensor applications.

The frequency response of the designed SMRs and the acoustic mirror performance have been analysed using the 1-D Mason model and a 2-D finite element model. Furthermore, a three dimensional finite element model of the devices has also been developed in order to estimate the sensitivity of these devices when exposed to fine particles of different size. Table I presents the main physical properties of the materials used for the modelling of the solidly mounted resonators. The density and acoustic velocity of Mo and SiO_2 are experimental values. Densities were determined using the X-ray reflectance method whereas the acoustic velocities were estimated using the $\lambda/2$ method as outlined by Olivares *et al*. [37]. The thicknesses of the thin films for the SMR designs working at 870 MHz and 1.5 GHz with Al electrodes and Au (with Cr adhesion layer) electrodes are summarised in Table II.

TABLE I. MATERIAL PROPERTIES USED IN THE SMRS MODELLING

MATERIAL	DENSITY (kg/m^3)	ACOUSTIC VELOCITY (m/s)
ZnO	5680	6330
Mo	10200	6280
SiO2	2170	5540
Al	2700	6450
Cr	7150	6630
Au	19300	3430
Si	2330	8320

TABLE II. THICKNESS OF THE LAYERS FOR THE SMR DESIGNS.

MATERIAL	THICKNESS	
	DESIGN 870 MHz	DESIGN 1.5 GHz
Mo	1.82 µm	1.05 µm
SiO2	1.65 µm	995 nm
ZnO	3.35 µm	1.85 µm
Al	200 nm	200 nm
ZnO	2.85 µm	1.35 µm
Cr	10 nm	10 nm
Au	100 nm	100 nm

3.1.1.Mason's Model

The 1-D Mason's model [38] was used in order to estimate the resonant frequency of the designed devices as well as the transmittance of the acoustic mirrors. Figure 3 shows the transmittance through the reflector stack as obtained with the one-dimensional Mason equivalent circuit based on the transmission line theory. Both reflectors show very low and similar transmittance around the desired centre frequencies whereas the bandwidth of the reflectors for 1.5 GHz resonators was found to be wider than the bandwidth for the 870 MHz reflectors. The impedance spectra of the designed

resonators were also evaluated using the Mason's analytical model. The obtained resonant frequencies with the Mason's model were found to be very close to the designed frequencies of 870 MHz and 1.5 GHz.

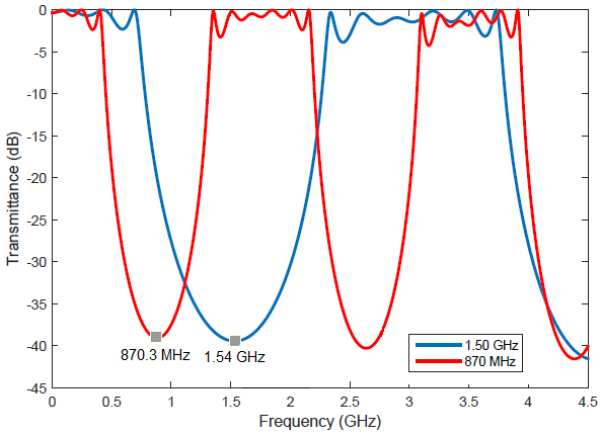

Figure 3. Simulated transmittance of the reflector stack consisting on 3 pairs of Mo/SiO_2 layers based on the Mason model.

3.1.2. *Two-dimensional finite element model*

A 2-D finite element analysis of the designed solidly mounted resonators was performed using the Acoustics Module of COMSOL Multiphysics software v4.4. A 2-D model of the SMRs was developed where the interaction between electrical potential and mechanical displacement in the resonators is solved by finite element method using the *pzd* interface in COMSOL software according to the following piezoelectric constitutive equations [39]

$$T_i = c_{ij}{}^E S_j - e_{ij} E_j \quad (2)$$

$$D_i = \mathcal{E}_{ij}{}^S E_j + e_{ij} S_j \quad (3)$$

T_i,c_{ij}, S_j ,e_{ij} ,E_j, D_i and $\mathcal{E}_{ij}$ are the stress components, the stiffness constants, the strain components, the piezoelectric stress constants, the electric field components, the electrical displacement components and the permittivity constants, respectively. The superscripts E and S denote that the constants are measured at a constant electric field and constant strain, respectively.

The 2-D finite element model (FEM) was used in order to evaluate the displacement profile of the waves in the resonator structure as well as the frequency response of the devices. This model used the 2-D plain strain assumption where the out of plane thickness is defined. Perfectly matched layers (PMLs) were used at the edges of the structure in order to account for the absorption of the elastic waves avoiding the reflection of waves at the boundaries of the geometry. The *ground* condition was applied to the bottom electrode ant the *electrical potential* was set to 1.0 V and applied to the top electrode. The *fixed constraint* condition was applied to the boundaries of the PML domains and all other boundaries were set as *free*. The meshing of this model was accomplished by using a mapped mesh with several distributions. The generated mesh consisted of an average of 4,500 domains elements.

A frequency domain analysis was performed in order to obtain the plots of impedance versus frequency of the SMRs. Figure 4 illustrates the impedance spectra of the SMRs as simulated with COMSOL software. From these simulation results, it can be observed that the frequency responses obtained with the 2-D FEM are similar to those obtained using the 1-D Mason's model. The frequency response of the 870 MHz design is very similar for the SMRs with Al and Au electrodes. However, unlike the results from the analytical model, the resonant frequency of the 1.5 GHz design varies slightly according to the electrode materials used. This could be explained as the finite element simulations used a 2-D model with finite electrode dimensions (200 µm).

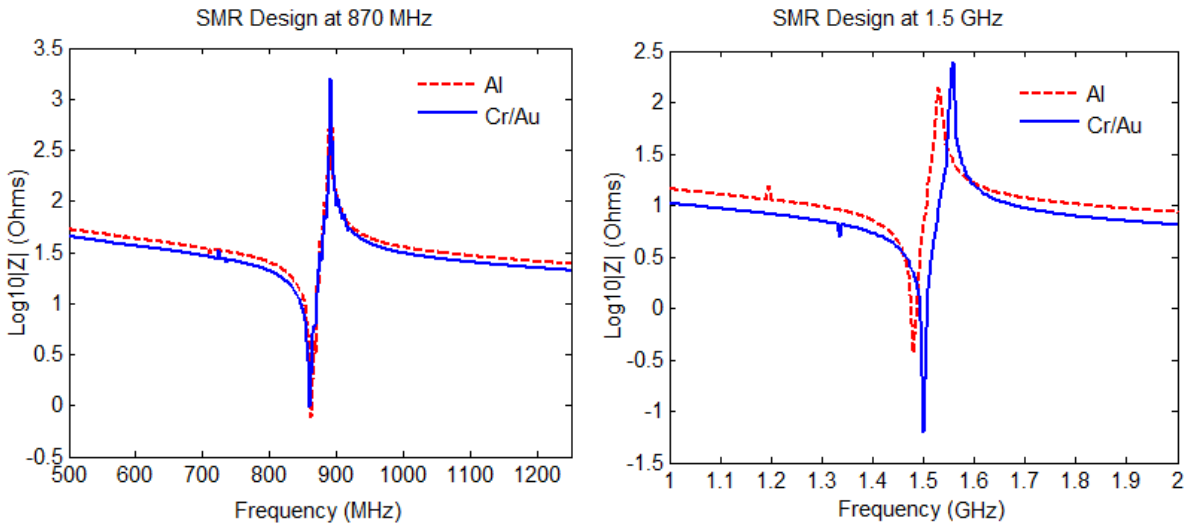

Figure 4. Frequency response of the designed SMRs modelled using a 2D finite element model.

Using the same 2D finite element model, the displacement profiles of the longitudinal waves of the SMRs were simulated at the resonant frequency. The standing wave amplitude as a function of depth into the SMRs [40] was also obtained by plotting the *y* component of the displacement field in the cross section of the device, confirming a good performance of the designed acoustic mirrors as the wave energy is confined within the resonator with practically no energy dissipating into the substrate. The displacement profile and standing wave of the SMR design with Al electrodes operating at 870 MHz are presented in Figure 5, which also illustrates the developed 2-D model of the devices.

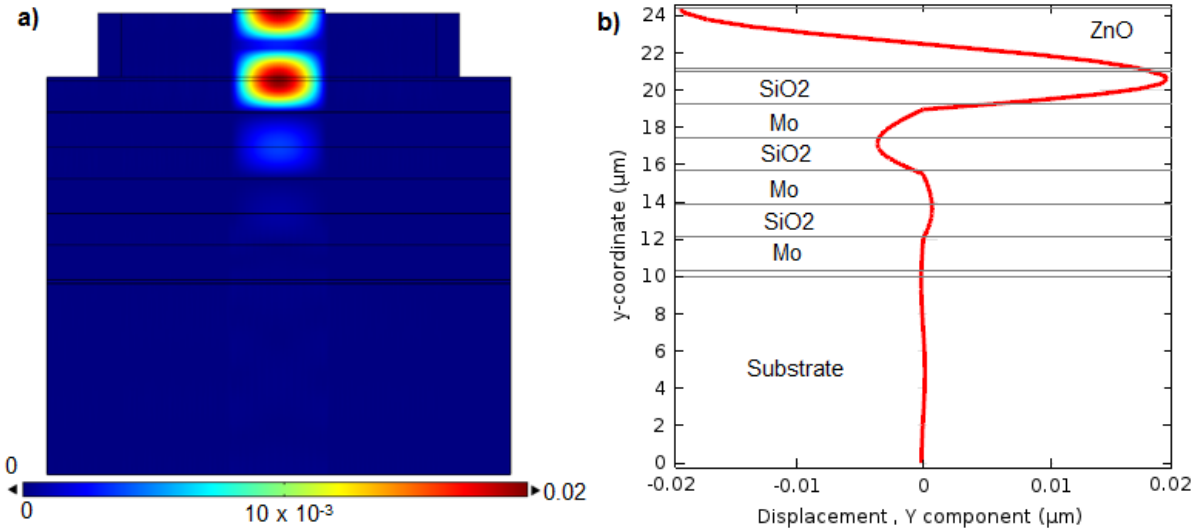

Figure 5. a) Displacement profile at resonant frequency, and b) standing wave amplitude as a function of depth of the 870 MHz SMR design obtained with the 2-D COMSOL model.

3.1.3. *Three-dimensional finite element model*

The 2D finite element model provides a very good approach for the evaluation of the frequency response of the SMRs. However, in order to evaluate the sensitivity of the SMR devices to the deposition of fine particles, a 3-D finite element model has been developed. The developed 3-D geometry consisted of only a quarter of the complete structure of the SMR so as to speed computation time and reduce computer memory usage. To this aim, the symmetry condition was applied to the appropriate boundaries and the electric and boundary conditions in this model were applied in a

similar way as previously explained for the 2-D model. The three dimensional model was also helpful to calculate the spurious responses of the SMRS.

As the 3-D geometry is formed by very thin layers, a swept mesh containing six elements and triangular mesh elements was used for meshing the model. In the electrodes area, a finer mesh was used compared to the rest of the model as this is the part where the acoustic wave mainly propagates. Figure 6(a) shows the meshed model composed by 28414 domain elements. The electrical impedance of the SMRs was simulated in COMSOL by computing the following expression using the *pzd* interface:

$$Z = \frac{V}{j\omega Q} \tag{4}$$

where Z is the electrical impedance, V is the voltage applied to the top electrode, ω is the angular frequency and Q is the total charge on the surface of the top electrode. The frequency response of the SMRs computed with the 3-D model is in accordance to that obtained with the 2-D model.

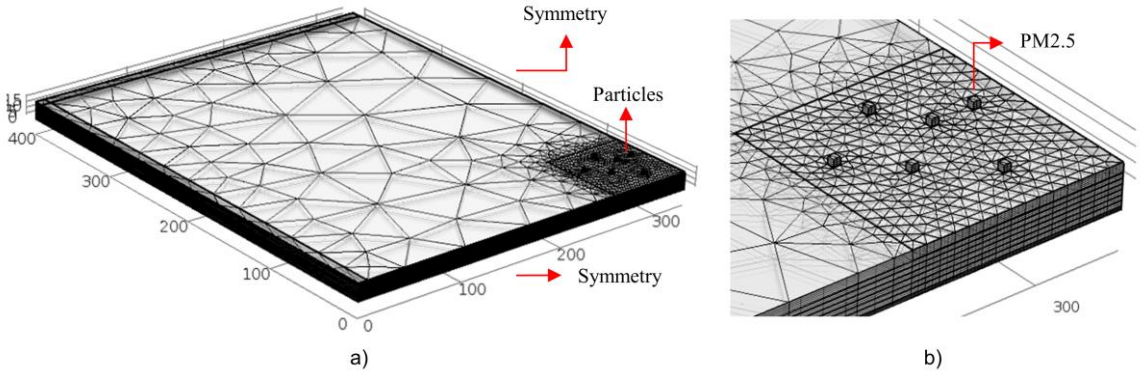

Figure 6. a) Developed 3-D finite element model of the SMR and b) particles deposited on the active area of the model.

The response of the SMRs to the deposition of particle matter was evaluated by using the developed 3-D finite element model. To this aim, PM2.5 and PM10 particles were simulated by placing cubic geometries on the sensing area of the SMRs, as shown in Figure 6(b). After the deposition of the particles, a frequency analysis of the models was again performed, showing that as the amount of particles on the sensing area increased, the simulated resonant frequency decreased. The computed frequency shifts were used to estimate the sensitivity of the SMRs. Figure 7 shows the estimated sensitivity of the modelled devices when detecting PM2.5 and PM10.

From the finite element simulation results, the mass sensitivity of the SMRs with Al electrodes was found to be slightly higher than the devices with gold electrodes when detecting both PM2.5 and PM10 and for both SMR designs working at 870 MHz and 1.5 GHz. This could be explained as the total mass of the gold top electrode is larger than that of the aluminium top electrode as suggested by Gabl [34]. It was observed that when detecting PM2.5 particles, the SMRs designed to work at a higher frequency (1.5 GHz) were estimated to have a greater sensitivity that the ones working at 870 MHz, demonstrating that the higher the resonant frequency, the higher the sensitivity of the device. However, when detecting PM10 the SMRs working at 870 MHz were found to have a greater mass sensitivity when compared to the 1.5 GHz devices. This could be explained by the influence of the penetration depth of the SMRs in their sensitivity. The results suggest that the amplitude of the frequency shift is determined by the fraction of the particle detected, i.e. penetrated by the acoustic wave as proposed in previous works [9, 41] . The 870 MHz device with a wavelength of ~7.3 µm would detect a bigger fraction of the PM10 particle compared to the 1.5 GHz device with a wavelength of ~4.22 µm hence a higher frequency shift is observed with the 870 MHz device when detecting PM10. Therefore, the resonant frequency of the SMR devices need to be taken into account when used as particle sensors in order to efficiently detect the particles. SMR devices with tailored

resonant frequencies may be used for the monitoring of airborne particles with different size distribution.

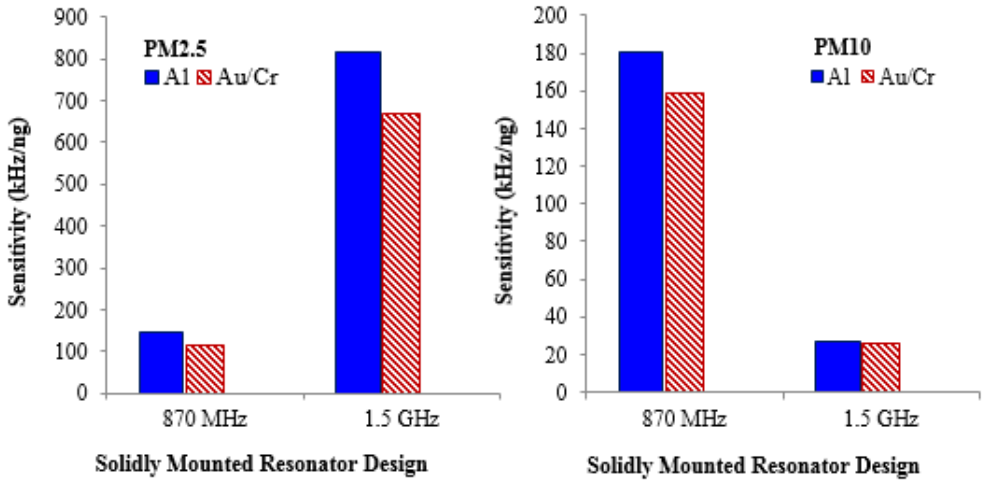

Figure 7. Estimated sensitivity of the designed Solidly Mounted Resonators with aluminium and gold/chromium electrodes working at 870 MHz and 1.5 GHz.

4. FABRICATION

The designed SMRs were fabricated on 4" p-type (100) silicon with 200 nm thermal oxide on either side. The different layers of the devices were deposited by RF sputtering or evaporation and patterned by a standard photolithography process using a total of 3 masks. The main steps of the fabrication process flow are shown in Figure 8.

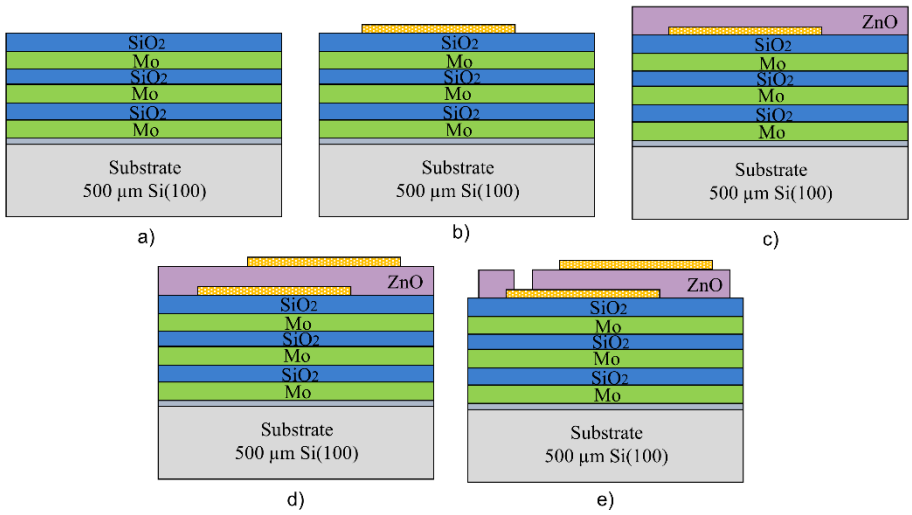

Figure 8. Schematic of the fabrication process flow of the designed SMR devices.

After the wafer cleaning process, three layers of Mo and three layers of SiO_2 were alternately sputtered on top of the Si substrate using a high target utilisation sputtering (HiTUS) system. The bottom electrode was then patterned with standard photolithography and the metal was thermally evaporated. The pattern was obtained with a lift-off process. The ZnO layer was reactively sputtered with the HiTUS system [42] using a 4-inch, 6mm thick Zn target and Ar/O_2 mixture, obtaining a deposition rate of ~20 nm/min. In the second mask process, the metal for the top electrode was deposited and patterned on the piezoelectric layer using the lift-off technique. Finally, the ZnO layer was patterned and a via was created through the piezoelectric layer in order to expose the bottom electrode for electrical contact by wet etching the ZnO in 2% glacial acetic acid and phosphoric acid

solution at room temperature. The deposition parameters of the piezoelectric and the acoustic mirror layers are summarised in Table III.

TABLE III. DEPOSITION PARAMETERS OF ZINC OXIDE, MOLYBDENUM AND SILICON DIOXIDE

PARAMETER	PIEZOELECTRIC	REFLECTOR LAYERS	
	ZnO	**Mo**	**SiO_2**
Deposition Method	RF reactive sputtering (HiTUS system)	RF sputtering (HiTUS system)	RF reactive sputtering (HiTUS system)
Target	Zn (99.999%)	Mo (99.999%)	Si (99.999%)
Base pressure (mbar)	$< 2 \times 10^{-6}$	$< 2 \times 10^{-6}$	$< 2 \times 10^{-6}$
Launch Power (W)	1000	1500	1000
Target Power (W)	800	1300	800
Ar flow rate (sccm)	55	60	55
O_2 flow rate (sccm)	41	0	8
Deposition Rate (nm/min)	~ 20	~30	~23

Figure 9(a) shows a cross-sectional SEM image of the acoustic mirror of the fabricated SMR device designed to operate at a resonant frequency of 870 MHz. The thicknesses of the reflector layers were estimated from the image and found to be within an acceptable range of the designed values. The thickness of the ZnO film was measured using a stylus profilometer, obtaining a reading of 2.96 µm and 2.35 µm or the 870 MHz design with Al and Au/Cr electrodes, respectively giving an error in the thicknesses of the piezoelectric layer of 13% and 21%. A top view of the fabricated devices with gold and aluminium electrodes are presented in Figures 9(b) and 9(c), respectively showing the ground planes and the square active area of 200 µm × 200 µm of the device, determined by the overlapping of the bottom and top electrodes.

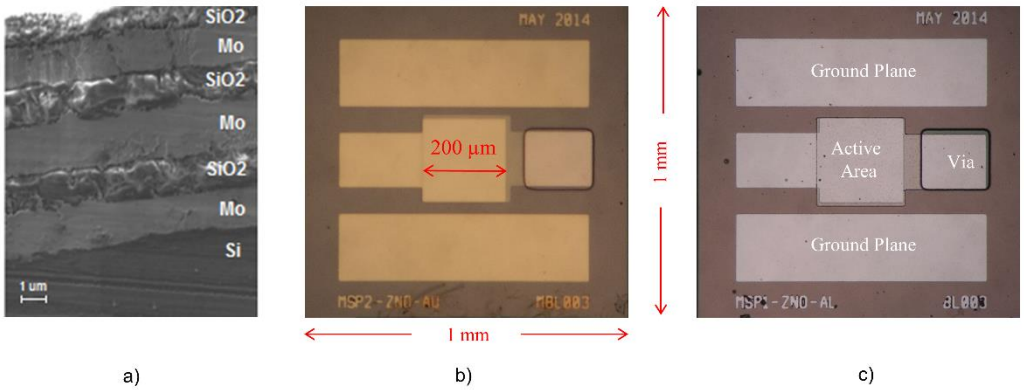

Figure 9. Fabricated devices: a) cross sectional view of the acoustic mirror and b) top view with Au/Cr electrodes and c) Al electrodes.

5. EXPERIMENTAL

For sensing applications, acoustic wave based devices are commonly used in an oscillator circuit configuration [43]. Physical properties produce a change in frequency, amplitude or phase of the acoustic wave which is associated to the property being measured. It is also important to take into account external disturbances to the device such as temperature and pressure effects since they induce undesirable changes on the wave path which are not directly related to the property being measured. For the suppression of these disturbances, a dual configuration is commonly used in which two identical acoustic wave devices are employed [22, 44], one acting as the reference channel and the other serving as the sensing device. The output directly associated to the property being sensed is given by the differential measurement of the oscillators. A typical frequency measurement configuration used with acoustic wave devices for sensing applications is shown in Figure 10.

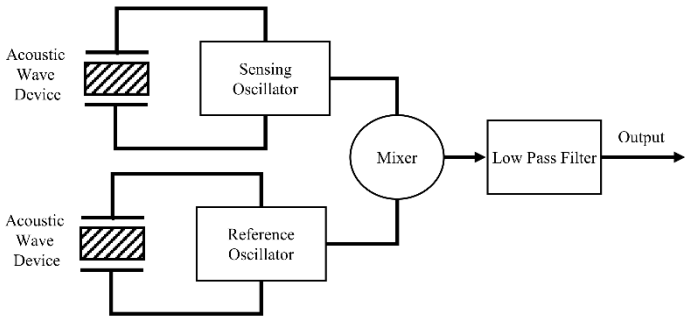

Figure 10. Frequency Measurement configurations of acoustic wave devices for particle sensing: block diagram of a dual configuration with mixing circuitry.

Initial characterisation of the fabricated devices in order to obtain the transmission characteristics was conducted using an Agilent Technologies E5071B network analyser with the device wire-bonded onto a testing board. Figure 11 shows the measured S_{11} parameter (reflection coefficient) of two of the SMR designs compared to the simulation results obtained with the 3D finite element model. For the SMR designed to operate at 870 MHz, the obtained series and parallel resonant frequencies of the fabricated devices were found to be 945 MHz and 972 MHz, respectively whereas the SMR designed to work at 1.5 GHz worked at a resonant frequency of ~1.7 GHz. A shift in the resonant frequency was observed between the modelled SMRs and the fabricated devices and this is discussed in the next section.

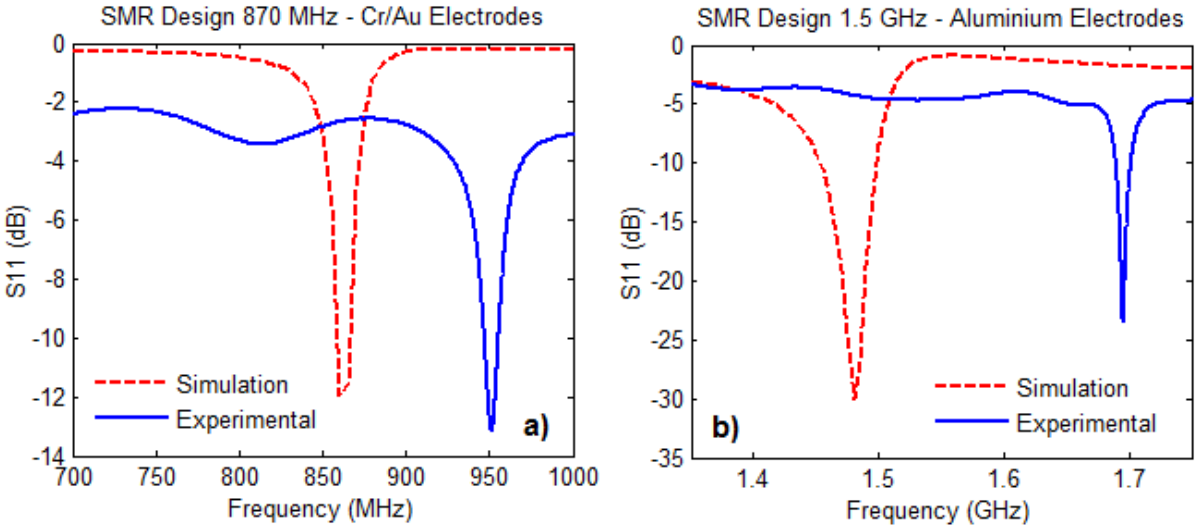

Figure 11. Experimental and Simulated reflection curves of the Solidly Mounted Resonators.

The fabricated SMRs were modelled by the Modified Butterworth Van Dyke circuit model (MBVD) [45] using the measured transmission (S_{21}) parameters. This model is a lumped element model which accounts for the losses in the electrodes and the piezoelectric layer. The equivalent model for the SMR working at ~970 MHz with aluminium electrodes was obtained using the equations presented in [46] and it is shown in Figure 12(a), where R_s represents the physical resistance of the top and bottom electrodes, R_m, C_m and L_m form the motional arm representing the mechanical resonance, C_0 is the electrical plate capacitance and R_0 represents the acoustic loss parasitic. With this equivalent model a fitted line of the measured characteristic was obtained and the series and parallel resonance frequencies of the SMRs can be calculated using (5) and (6).

$$f_s = \frac{1}{2\pi\sqrt{L_m C_m}} \tag{5}$$

$$f_p = f_s \sqrt{\frac{C_m + C_0}{C_0}} \tag{6}$$

For the experimental measurements, the SMR devices with aluminium electrodes working at a resonant frequency of ~970 MHz were driven by a Colpitts type oscillator circuit shown in Figure 12(b). The SMRs were operated in a dual configuration in order to eliminate common mode variations, in which one sensor operated as the reference and the other one as the actual sensing device. The output differential signal of the system was acquired and logged to a PC using a microcontroller.

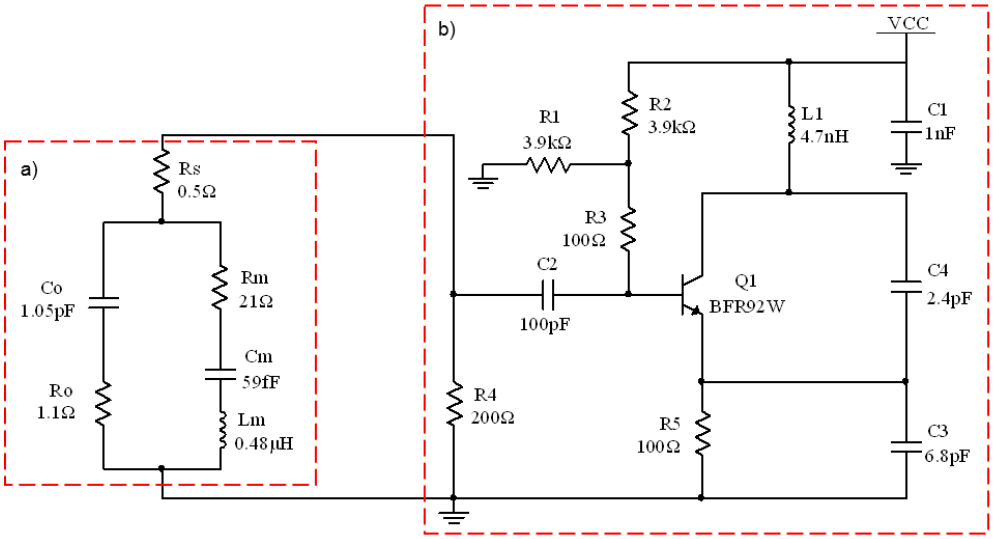

Figure 12. Schematic of the SMR driven by a Colpitts type oscillator: a) Modified Butterworth Van Dyke model of the SMR working at ~970 MHz and b) simplified Colpitts oscillator circuitry.

Preliminary testing was performed in order to evaluate the response of the fabricated SMRs to the deposition of fine particles. To this aim, PTFE particles of 1 µm in size were deposited onto the active area of the resonator. In this preliminary stage, the deposition of particles was carried out in a similar way to that reported in [9] and the frequency shift was monitored. Fig. 13(a) shows the particles deposited on the active area of the SMR: some individual particles along the surface and a bigger clump of the particles in the centre. A typical frequency response is shown in Figure 13(b). The devices responded to the mass loading of the particles as a negative frequency shift was observed when the particles were deposited, obtaining a sensor responsivity of ~220 kHz/ng.

A particle sensor system was developed using the fabricated solidly mounted resonators operating at 970 MHz. This sensor system was characterised inside an environmental chamber, where the SMR-based sensor was placed together with reference commercial sensor GRIMM 1.107 monitor (GRIMM Technologies, Inc.) for the measurement of particle concentration inside the chamber. Test particles were injected into the chamber and the real-time response of all sensors was recorded. Details on the oscillator circuit design, the developed particle sensor system and the experimental setup are reported elsewhere [47]. Target particles included Arizona dust (Powder Technology Inc.) and Dolomite powder with nominal particle size of 0-3 µm and 0.2-30 µm, respectively. Figure 14 shows the response of the SMR-based sensor when the test particles were injected. For the same particle concentration of ~60 mg/m^3 as measured by the optical particle counter (Grimm technologies Inc.), the SMR-based sensor showed a frequency shift of ~315 kHz when exposed to Arizona dust and ~75 kHz when exposed to Dolomite powder. The sensitivity of the sensor was found to be 5.25 kHz per mg/m^3 when detecting fine particles of 0-3 µm. However, when detecting particles with larger diameter (0.2-30 µm) a lower sensitivity of 1.25 kHz per mg/m^3 was observed.

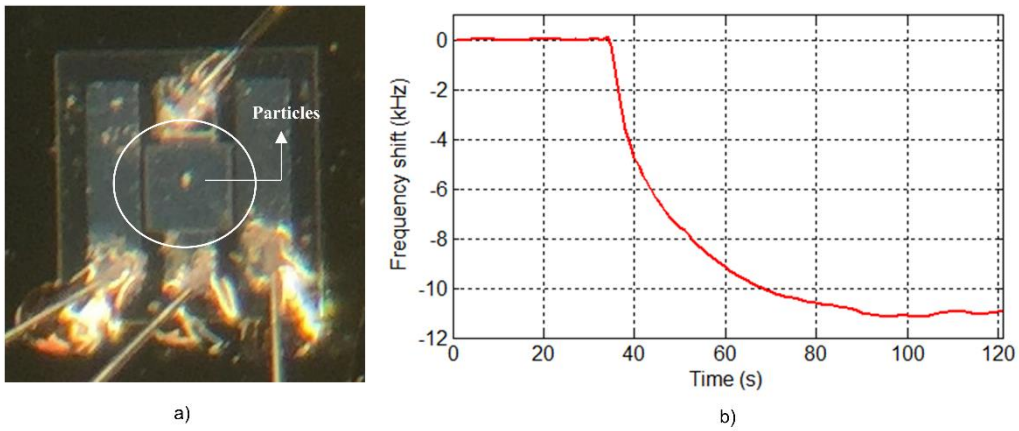

Figure 13. Preliminary experimental particle testing: a) Particles of 1 μm in size deposited on the sensing area of the fabricated SMR devices and b) the measured frequency shift due to the particle deposition onto the resonator.

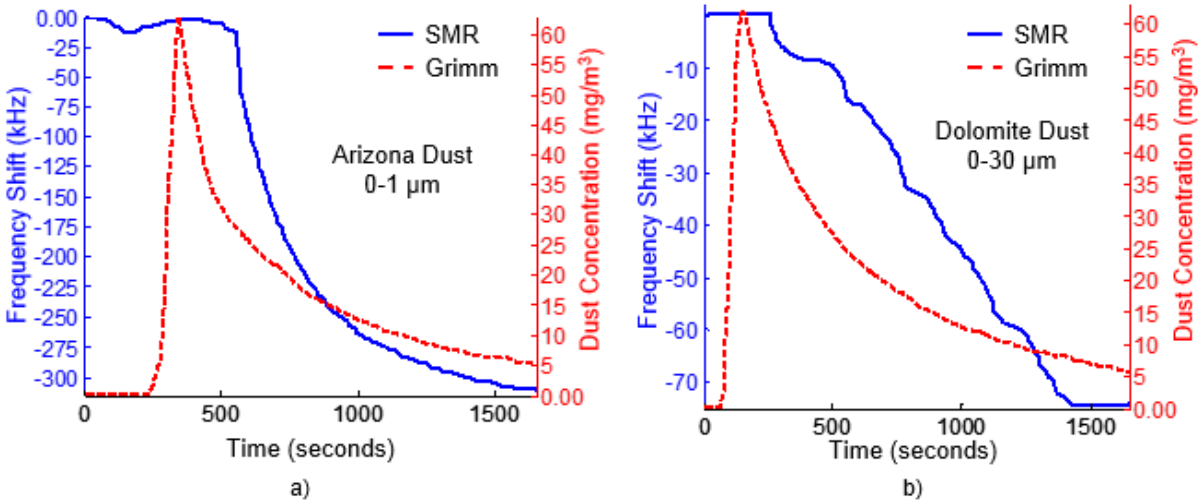

Figure 14. Frequency response of the SMR particle sensor system to the deposition of a) Arizona dust and b) Dolomite powder.

6. DISCUSSION

From the device characterisation results, it was noticed that the experimentally measured resonant frequencies (970 MHz and 1.7 GHz) of the fabricated devices was approximately 10% higher compared to the theoretically designed values obtained from the 1-D model and the finite element analysis (870 MHz and 1.5 GHz). The main reason of these frequency variations is a discrepancy between the nominal thickness of the piezoelectric layers and the actual thickness of the deposited ZnO films. This is attributed to a reduction in the sputtering rate of the ZnO during the fabrication process which lead to the deposition of thinner layers (variation of 10%) than desired, explaining the greater resonant frequencies measured. The thickness of the piezoelectric layer is critical when designing film bulk acoustic devices as this mainly determines the resonant frequency of the device. The thicknesses of the deposited acoustic mirror layers are within an acceptable range to provide a large enough bandwidth and confine the acoustic wave within the fabricated resonators.

Another important error factor to consider when comparing the experimental to the theoretical results is that the properties of the materials used for the finite element simulations were those found in the literature. These values can considerably differ to the actual values of the deposited ZnO films as the crystalline quality and electrical properties strongly depend on the deposition technique and the

thickness of the layer [48]. With the actual thicknesses measured of the fabricated devices, a new finite element model was developed for the SMRs working at 970 MHz with both aluminium and gold electrodes. The estimated resonant frequencies of the new models were found to be in agreement with the experimental ones.

The experimental sensitivity of the 970 MHz SMR with aluminium electrodes was found to be higher than the sensitivity estimated from the finite element analysis. This was expected as the fabricated SMRs resonate at a higher frequency compared to that of the designed devices, showing how as the resonant frequency of the device increases, the sensitivity increases as well. New simulations were performed in order to estimate the sensitivity of the 970 MHz device, which showed a similar value to that obtained in the preliminary experimental results.

7. CONCLUSIONS

High frequency solidly mounted resonators have been designed, modelled and fabricated for the development of a smart particle sensor system. The frequency response of the devices, the performance of the acoustic mirror and their sensitivity when detecting particulate matter were estimated by means of finite element analysis. The designed devices were fabricated in a 5 masks process and the experimental resonant frequencies were found to be ~970 MHz and ~1.7 GHz. From the preliminary experiments, a high sensitivity of 220 kHz/ng was exhibited by the 970 MHz SMR device when detecting PM2.5 Current work is under progress for the development of a miniature and low power smart sensor system based on the fabricated SMRs for the real-time and low-cost monitoring of airborne particulate matter by the full integration of the SMR with CMOS technology.

ACKNOWLEDGEMENTS

This work was funded under the European Commission 7th Framework Programme, Project No. 611887, "Multi-Sensor-Platform for Smart Building Management: MSP". F.H.Villa-Lopez thanks the financial support from the National Mexican Council of Science and Technology (CONACYT). G. Rughoobur wishes to acknowledge financial support from the Cambridge Trusts.

REFERENCES

[1] Rückerl, R., Schneider, A., Breitner, S., Cyrys, J. and Peters, A., *Health effects of particulate air pollution: A review of epidemiological evidence.* Inhalation Toxicology, 2011. **23**(10): p. 555-592.

[2] Martinelli, N., Olivieri, O. and Girelli, D., *Air particulate matter and cardiovascular disease: A narrative review.* European Journal of Internal Medicine, 2013. **24**(4): p. 295-302.

[3] Lim, H. H., Park, D., Maeng, J. Y., Hwang, J. and Kim, Y. J. *MEMS Based Integrated Particle Detection Chip for Real Time Environmental Monitoring*. *19th IEEE International Conference on Micro Electro Mechanical Systems (MEMS)*, 2006.

[4] Hajjam, A., Wilson, J. C., Rahafrooz, A. and Pourkamali, S. *Fabrication and characterization of resonant aerosol particle mass sensors*. *IEEE 23rd International Conference on Micro Electro Mechanical Systems (MEMS)*, 2010.

[5] Mehdizadeh, E., Kumar, V., Pourkamali, S., Gonzales, J. and Abdolvand, R. *A two-stage aerosol impactor with embedded MEMS resonant mass balances for particulate size segregation and mass concentration monitoring*. *IEEE Sensors Conference*, 2013. Baltimore, MD.

[6] Wasisto, H. S., *et al. A resonant cantilever sensor for monitoring airborne nanoparticles*. *16th International Solid-State Sensors, Actuators and Microsystems Conference (TRANSDUCERS)* 2011. Beijing, China.

[7] Chuan, R. L., *An instrument for the direct measurement of particulate mass.* Journal of Aerosol Science, 1970. **1**(2): p. 111-113.

[8] Bowers, W. D. and Chuan, R. L., *Surface acoustic-wave piezoelectric crystal aerosol mass microbalance.* Review of Scientific Instruments, 1989. **60**(7): p. 1297-1302.
[9] Thomas, S., Racz, Z., Cole, M. and Gardner, J. W. *Dual high-frequency Surface Acoustic Wave Resonator for ultrafine particle sensing*. *IEEE Sensors Conference*, 2013.
[10] Paprotny, I., Doering, F., Solomon, P. A., White, R. M. and Gundel, L. A., *Microfabricated air-microfluidic sensor for personal monitoring of airborne particulate matter: Design, fabrication, and experimental results.* Sensors and Actuators A: Physical, 2013. **201**(0): p. 506-516.
[11] Paprotny, I., Doering, F. and White, R. M. *MEMS Particulate Matter (PM) monitor for cellular deployment*. *IEEE Sensors Conference*, 2010.
[12] García-Gancedo, L., *et al.*, *AlN-based BAW resonators with CNT electrodes for gravimetric biosensing.* Sensors and Actuators B: Chemical, 2011. **160**(1): p. 1386-1393.
[13] He, X. L., Garcia-Gancedo, L., Jin, P.C., Zhou, J., Wang, W.B., Dong, S.R., Luo, J.K., Flewitt, A.J., and Milne, W.I., *Film bulk acoustic resonator pressure sensor with self temperature reference.* Journal of Micromechanics and Microengineering, 2012. **22**(12).
[14] Clayton, L. D. and EerNisse, E. P., *Quartz thickness-shear mode pressure sensor design for enhanced sensitivity.* IEEE Transactions on Ultrasonics, Ferroelectrics and Frequency Control, 1998. **45**(5): p. 1196-1203.
[15] Thomas, S., Cole, M., de Luca, A., Torrisi, F., Ferrari, A. C., Udrea, F. and Gardner, J. W. *Graphene-coated Rayleigh SAW resonators for NO2 detection*. *Eurosensors*, 2014. Brescia, Italy.
[16] Nirschl, M., *et al.*, *Film bulk acoustic resonators for DNA and protein detection and investigation of in vitro bacterial S-layer formation.* Sensors and Actuators A: Physical, 2009. **156**(1): p. 180-184.
[17] Cole, M., Spulber, I. and Gardner, J. W., *Surface acoustic wave electronic tongue for robust analysis of sensory components.* Sensors and Actuators B: Chemical, 2015. **207, Part B**(0): p. 1147-1153.
[18] Yang, J., Rácz, Z., Gardner, J. W., Cole, M. and Chen, H., *Ratiometric info-chemical communication system based on polymer-coated surface acoustic wave microsensors.* Sensors and Actuators B: Chemical, 2012. **173**(0): p. 547-554.
[19] Cole, M., Covington, J. A. and Gardner, J. W., *Combined electronic nose and tongue for a flavour sensing system.* Sensors and Actuators B: Chemical, 2011. **156**(2): p. 832-839.
[20] Vivancos, J.-L., Rácz, Z., Cole, M. and Gardner, J. W., *Surface acoustic wave based analytical system for the detection of liquid detergents.* Sensors and Actuators B: Chemical, 2012. **171–172**: p. 469-477.
[21] Drafts, B., *Acoustic wave technology sensors.* IEEE Transactions on Microwave Theory and Techniques, 2001. **49**(4): p. 795-802.
[22] Thomas, S., Racz, Z., Cole, M. and Gardner, J. W., *High-frequency One-port Colpitts SAW Oscillator for Chemical Sensing.* Proceedings of the The Sixth International Conference on Advances in Circuits, Electronics and Micro-electronics (CENICS), 2013: p. 13-17.
[23] Gardner, J. W., Varadan, V.K., and Awadelkarim, O.O., *Microsensors, MEMS, and Smart Devices*, ed. John Wiley & Sons Ltd. 2001.
[24] Sauerbrey, G., *Verwendung von Schwingquarzen zur Wägung dünner Schichten und zur Mikrowägung.* Zeitschrift für Physik 1959. **155**: p. 206-222.
[25] Campanella, H., *Acoustic Microresonator Technologies*, in *Acoustic Wave and Electromechanical Resonators : Concept to Key Applications*. 2010, Artech House: Norwood.
[26] Newell, W. E., *Face-mounted piezoelectric resonators.* Proceedings of the IEEE, 1965. **53**(6): p. 575-581.
[27] Bi, F. Z. and Barber, B. P., *Bulk acoustic wave RF technology.* IEEE Microwave Magazine, 2008. **9**(5): p. 65-80.
[28] Qiliang, Z., Lec, R. M. and Pourrezaci, K., *The study of an interaction of solid particles with various surfaces using TSM sensors.* Ultrasonics, Ferroelectrics, and Frequency Control, IEEE Transactions on, 2006. **53**(1): p. 167-174.
[29] Dybwad, G. L., *A sensitive new method for the determination of adhesive bonding between a particle and a substrate.* Journal of Applied Physics, 1985. **58**(7): p. 2789-2790.

[30] Pomorska, A., Shchukin, D., Hammond, R., Cooper, M. A., Grundmeier, G. and Johannsmann, D., *Positive Frequency Shifts Observed Upon Adsorbing Micron-Sized Solid Objects to a Quartz Crystal Microbalance from the Liquid Phase.* Analytical Chemistry, 2010. **82**(6): p. 2237-2242.

[31] Johannsmann, D., *The quartz crystal microbalance in soft matter research : fundamentals and modeling*. 2014: Springer.

[32] Johannsmann, D., Reviakine, I. and Richter, R. P., *Dissipation in Films of Adsorbed Nanospheres Studied by Quartz Crystal Microbalance (QCM).* Analytical Chemistry, 2009. **81**(19): p. 8167-8176.

[33] Kanbara, H., Kobayashi, H. and Nakamura, K., *Analysis of Piezoelectric Thin Film Resonators with Acoustic Quarter-Wave Multilayers.* Japanese Journal of Applied Physics, 2000. **39**(5B): p. 3049-3053.

[34] Gabl, R., *et al. Novel integrated FBAR sensors: a universal technology platform for bio- and gas-detection. Proceedings of IEEE Sensors,* 2003.

[35] Enjamuri, S., Amsanpally, A. and Raju, K. C. J. *Optimization and analysis of piezoelectric and electrode materials' thickness effects on the performance of film bulk acoustic resonator*. *1st International Symposium on Physics and Technology of Sensors (ISPTS),* 2012.

[36] Salgar, S., Guntae, K., Dae-Hyun, H. and Kim, B. *Modeling and simulation of the thin film bulk acoustic resonator*. *Frequency Control Symposium and PDA Exhibition, 2002. IEEE International*, 2002.

[37] Olivares, J., Wegmann, E., Capilla, J., Iborra, E., Clement, M., Vergara, L. and Aigner, R., *Sputtered SiO2 as low acoustic impedance material for Bragg mirror fabrication in BAW resonators.* IEEE Transactions on Ultrasonics, Ferroelectrics, and Frequency Control, 2010. **57**(1): p. 23-29.

[38] Rosenbaum, J., *Bulk Acoustic Wave Theory and Devices*. 1988, Norwood, MA: Artech House.

[39] Ballentine, D. S., White, R. M., Martin, S. J., Ricco, A. J., Zellers, E. T., Frye, G. C. and Wohltjen, H., *Acoustic wave sensors: theory, design and physico-chemical applications*, ed. Academic Press. 1997, San Diego.

[40] Lakin, K. M. B., J.; McDonald, J. F.; McCarron, K.T. *Improved bulk wave resonator coupling coefficient for wide bandwidth filters*. *IEEE Ultrasonics Symposium,* 2001.

[41] Nirschl, M., Schreiter, M. and Vörös, J., *Comparison of FBAR and QCM-D sensitivity dependence on adlayer thickness and viscosity.* Sensors and Actuators A: Physical, 2011. **165**(2): p. 415-421.

[42] García-Gancedo, L., Pedrós, J., Zhu, Z., Flewitt, A. J., Milne, W. I., Luo, J. K. and Ford, C. J. B., *Room-temperature remote-plasma sputtering of c-axis oriented zinc oxide thin films.* Journal of Applied Physics, 2012. **112**(1): p. 014907.

[43] Vellekoop, M. J., Nieuwkoop, E., Haartsan, J. C. and Venema, A. *A Monolithic SAW Physical-Electronic System for Sensors*. *IEEE Ultrasonics Symposium,* 1987.

[44] Jeutter, D., Josse, F., Johnson, M., Wenzel, M., Hossenlopp, J. and Cernosek, R. *Design of a portable guided SH-SAW chemical sensor system for liquid environments*. *Proceedings of the 2005 IEEE International Frequency Control Symposium and Exposition,*, 2005.

[45] Larson, J. D., III, Bradley, R. C., Wartenberg, S. and Ruby, R. C. *Modified Butterworth-Van Dyke circuit for FBAR resonators and automated measurement system*. *IEEE Ultrasonics Symposium,* 2000.

[46] Chatras, M., *et al.*, *Modeling and Design of BAW Resonators and Filters for Integration in a UMTS Transmitter*, in *Modeling and Measurement Methods for Acoustic Waves and for Acoustic Microdevices*. 2013, InTech.

[47] Thomas, S., Villa-López, F. H., Theunis, J., Peters, J., Cole, M. and Gardner, J. W., *Particle Sensor System using Solidly Mounted Resonators*, submitted to IEEE Sensors Journal, Editor. 2015.

[48] Jae-Min, M., Wook, H. Y., Dong-Hi, L., Ilgu, Y., Sang, H. B. and Sang-Yeol, L., *Effects of Thickness Variation on Properties of ZnO Thin Films Grown by Pulsed Laser Deposition.* Japanese Journal of Applied Physics, 2002. **41**(1R): p. 28.